



Performance of concrete produced with alkali-activated artificial aggregates

Gopal Bharamappa Bekkeri¹ · Kiran K. Shetty¹ · Gopinatha Nayak¹

Received: 16 July 2023 / Accepted: 13 March 2024 / Published online: 5 April 2024
© The Author(s) 2024

Abstract

The excessive use of natural aggregates raises mining activity. Further, it leads to environmental damage, which can be reduced using artificial aggregates produced from waste powdered materials. This study discussed the production process of alkali-activated artificial coarse aggregates and how their use affects the behavior of concrete. The different concrete mixtures were designed by replacing natural aggregates with artificial ones at different percentages. Various tests were conducted to determine concrete's fresh, hardened, permeability, and microstructural characteristics. The result showed that concrete incorporated with artificial aggregates can achieve higher workability and lower density than natural aggregate concrete. The mechanical strengths were slightly decreased as the percentage addition of artificial aggregates in a mix increased. However, adding up to 50% showed comparable results to natural aggregate concrete. The water permeability and chloride ion penetration were within the standard limits for all the mixes. The scanning electron micrographs showed a solid and compact ITZ between the phases. XRD pattern revealed that the addition of artificial aggregates had not changed the mineralogical composition of the concrete; the formation of hydrated products helps concrete obtain strength. The study concluded that artificial aggregates could effectively replace natural coarse aggregate in producing structural concrete with many advantages.

Keywords Artificial aggregate concrete · Alkali-activated artificial aggregates · Pelletization · Seashell powder · Ground granulated blast furnace slag · Fly ash

Introduction

The concrete contains 70–80% aggregates, 12–14% cement, and 8–10% water by mass. To make concrete of 1 m³ quantity, approximately two tons of aggregates are needed. The demand for construction aggregates has increased every year across the world. A recent statistical study reported that the worldwide demand for aggregates was 51.7 billion metric tons in 2018 and is expected to enlarge by 5.2% yearly. Whereas, in India, the use of aggregates was more than 5 billion metric tons in the year 2020, and further, it is increasing every year due to increased construction and infrastructure development activities [1–6]. In this rapid growth, the utilization of natural aggregates has stretched out to an alarming level that leads to severe environmental hazards [1–4, 7–9].

Many countries have introduced policies and regulations to mitigate the environmental risks due to the overexploitation of natural resources to get natural aggregates and care for their scarcity. Hence, finding an alternative material to natural aggregates is necessary to keep the environment healthy [2, 3, 7, 9]. On the other side, a massive amount of waste is generated from various sectors, and less quantity of this is used for various purposes. In most countries, industrial wastes remain unutilized, and disposal or landfilling of them has a considerable impact on the environment, including water and air pollution [3, 4, 7, 10–13].

In the past two decades, aggregates were produced artificially using wastes generated from different industrial sectors. Producing these artificial aggregates makes it possible to resolve issues associated with waste recycling and the scarcity of natural aggregates [7, 9, 14, 15]. The artificial aggregates can be prepared using various methods such as pelletization, crushing, mold casting, and hand shaping [7, 16]. It is found that most of the researchers have used the pelletization method to prepare the artificial aggregates, and this method requires disk pelletizer

✉ Kiran K. Shetty
kiran.shetty@manipal.edu

¹ Department of Civil Engineering, Manipal Institute of Technology, Manipal Academy of Higher Education, Manipal, Karnataka 576104, India

equipment [17–19]. Besides, producing artificial aggregates requires either of two basic techniques: cold bonded or sintering [20]. In the cold bonded technique, the aggregates are produced using cementitious materials to bind the waste materials at temperatures lower than 100 °C [10, 18, 19, 21, 22]. The sintering technique produces the aggregates using high temperatures (above 1000 °C) to solidify the aggregate pellets by fusing waste material particles [10, 18, 19, 21, 23–27]. The aggregates obtained from the cold bonded technique are always sustainable and environmentally friendly compared to those produced from the sintering technique since heat-cured aggregates involve more energy consumption and corresponding carbon dioxide emission [4, 8, 14, 25, 28, 29]. However, one of the significant advantages of sintered aggregates is that they provide good strength in a short period, so they can be used immediately after production, unlike cold bonded aggregates requiring long days to attain strength through a curing process [10]. However, the aggregates produced from both methods are lightweight. Hence, using these aggregates makes it possible to make lightweight concrete, which results in the economical design of structural components [10, 15, 28].

Many researchers have studied cementitious-based artificial aggregate preparation using industrial wastes through sintering and cold-bonded methods. Nevertheless, in these aggregates, it was observed that more water absorption led to corresponding concrete porous. Hence, to overcome this drawback to a lower level and make it more sustainable, the alkali activation method has been introduced to produce artificial aggregates. The production of alkali-activated aggregates requires rich alumina-silica content waste materials and alkali activators like Na_2SiO_3 , K_2SiO_3 , NaOH , and KOH [8, 9, 14]. Therefore, producing these alkali-activated aggregates makes it feasible to enhance physicomechanical and durability properties to some extent.

Therefore, in this study, cold-bonded alkali-activated artificial aggregates named as artificial coarse aggregates (ACA) were produced by blending fly ash (FA), ground granulated blast furnace slag (GGBS), and seashell powder (SSP). This study aims to produce M-40 grade concrete by incorporating ACA for different replacement levels with natural coarse aggregates (NCA). The fresh, hardened, and microstructural properties of concrete for different mixes were characterized. The experiments conducted to investigate the concrete qualities include workability, density, compressive strength (CS), split tensile strength (STS), flexural strength (FS), ultrasonic pulse velocity test (UPV), water permeability, and rapid chloride penetration test (RCPT). The correlations between the properties above were also presented and discussed. The microstructure characteristics were analyzed using scanning electron microscopy (SEM) and X-ray diffraction (XRD).

Significance of the study

Employing waste materials to manufacture artificial aggregates has an exciting future because there is a growing interest in and demand for recycling waste products. This study targets to produce artificial aggregates using seashell powder as a novel raw material along with FA and GGBS to conserve natural resources and reduce aggregate mining activities that harm the environment. Due to economic and environmental factors, the production of artificial aggregates and their use in manufacturing new concrete has been gradually rising. However, there is currently a dearth of knowledge on the quality of concrete with artificial aggregate. Further, this study aims to investigate the effects of synthetic aggregate on the characteristics of freshly poured and fully cured concrete. Overall, it provides essential information for the practical application of artificial aggregate in forming fresh concrete.

Experimental program

Production of artificial aggregates

The FA, GGBS, and SSP were utilized to produce alkali-activated artificial aggregates. FA was procured from the Udupi Power Corporation Limited, Udupi district of Karnataka state. It was finer than 75 μm with minor breakable lumps. It was examined as per IS 3812 (Part 1)- 2013 [30]. The GGBS was collected from Astra Chemicals, Tamil Nadu, India. The SSP of significantly finer size obtained by processing involves the collection of waste seashells, cleaning, crushing, and grinding. Table 1 lists the physico-chemical characteristics of FA, GGBS, and SSP. Figure 1 demonstrates SEM micrographs of all the raw materials and observed that the FA particles were of rounded shape, GGBS particles were of an angular shape, and SSP particles exhibited multi-layered hierarchical structure formed by stacking many similar flakes along parallel orientations. A 10 M sodium hydroxide (NaOH) solution and a sodium silicate (Na_2SiO_3) solution of commercial quality, including 8.04% Na_2O , 26.20% SiO_2 , and 65.76% H_2O by weight, were used as an activator to form artificial aggregates. 400 g of NaOH flakes were dissolved in a liter of distilled water to prepare the 10 M NaOH solution, which was then used after twenty-four hours.

The pelletization method manufactured the artificial aggregates and solidified them at room temperature to obtain artificial aggregates at the lowest possible cost and energy consumption. The artificial aggregates in the form of pellets were produced using disk pelletizer equipment,

Table 1 Properties of raw materials

Properties	Item	FA	GGBS	SSP
Physical properties	Specific gravity	2.24	2.85	2.36
	Specific surface area (m ² /g)	1.55	0.51	3.65
Chemical properties	SiO ₂	51.67	35.370	0.85
	Al ₂ O ₃	21.62	18.03	0.21
	CaO	3.90	33.05	74.00
	Fe ₂ O ₃	12.70	0.36	0.29
	MgO	1.20	7.73	0.17
	Na ₂ O	1.97	2.984	1.10
	K ₂ O	1.81	0.232	0.075
	P ₂ O ₅	0.374	0.739	–
	TiO ₂	1.32	0.8	0.015
	SO ₃	0.66	0.012	–
	MnO	0.081	0.12	–
	Cl	0.024	0.009	–
	Loss on ignition	2.15	0.26	–

as shown in Fig. 2. The disk pelletizer used is 500 mm diameter and 100 mm depth, and it has speed and angle variations from 1–65 rpm to 0°–90°, respectively. In a study for the preparation of aggregates, the angle and speed were maintained at 45° and 45 rpm, respectively. The pelletization duration was maintained for 20 min. The overall procedure of fresh pellets production is as follows: (1) Dry mixing of the calculated quantity of raw materials, (2) Sprinkling alkaline solution of the estimated quantity, (3) Collection of fresh pellets, and (4) Air curing of fresh pellets for one day to attain initial strength followed by ambient curing for 28 days. The surfaces of the freshly collected aggregate pellets were treated with the same alkaline solution of 10 M concentration by spraying method to improve the properties. Figure 3 represents an overall production procedure of alkali-activated artificial aggregates.

In a study, different trial mixes were made to produce good-quality artificial aggregates comparable to natural aggregates. The parameters, including pelletization

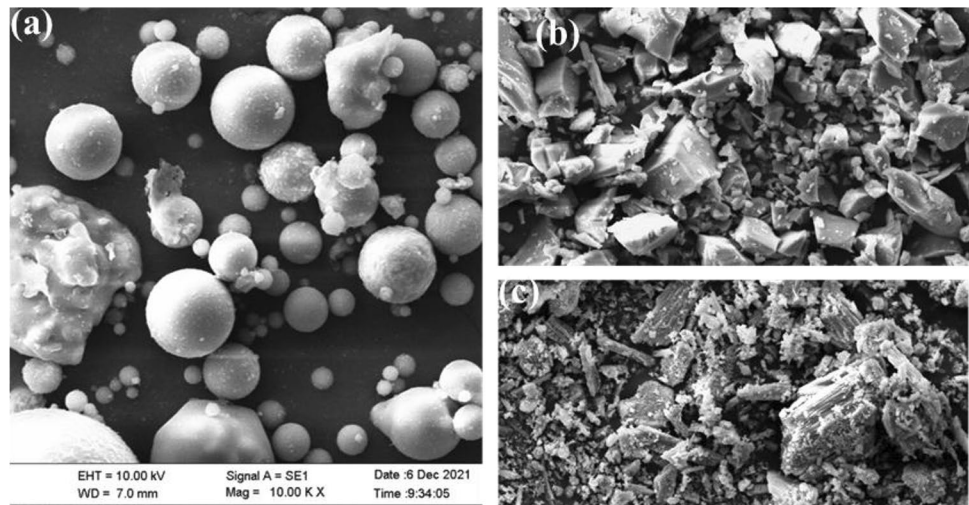
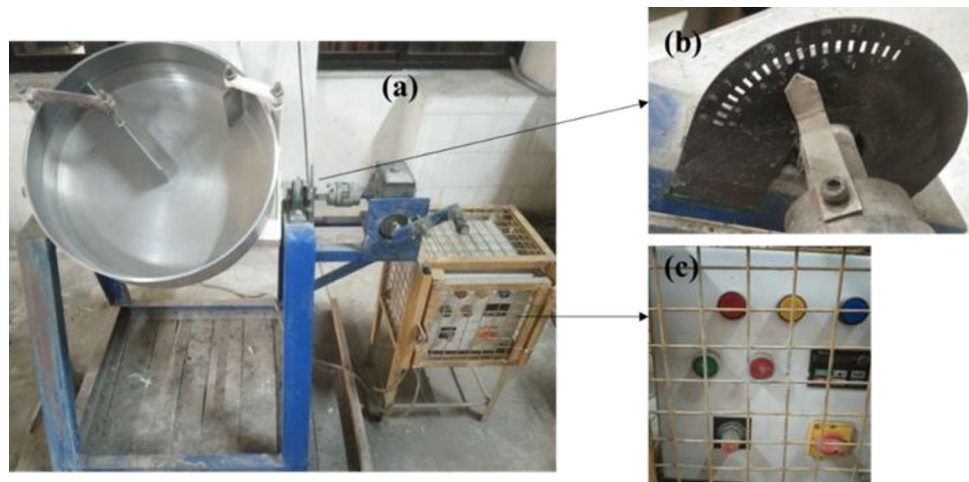
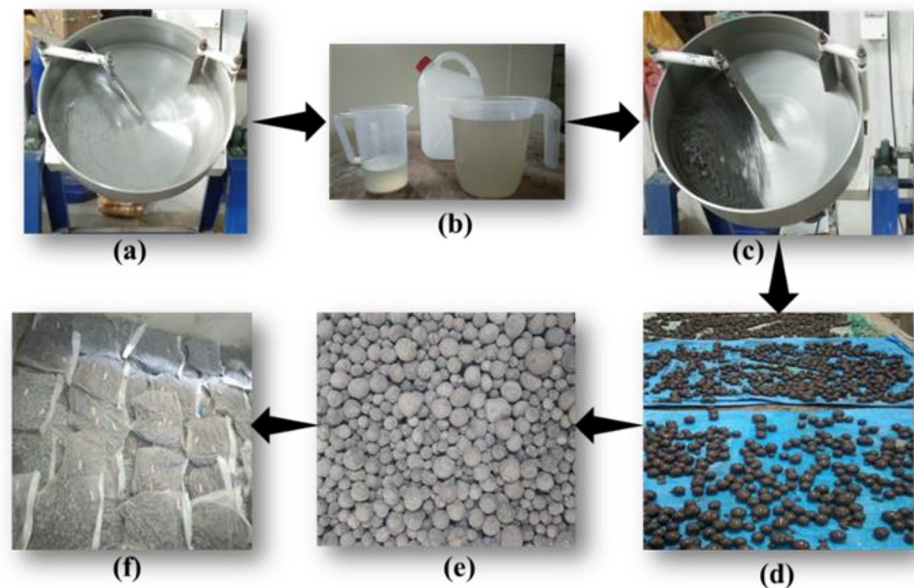
Fig. 1 SEM micrographs of raw materials **a** FA, **b** GGBS, **c** SSP**Fig. 2** Pelletizer equipment **a** Overall disk pelletizer setup, **b** Stretched view of angle setup, **c** Stretched view of speed controller setup

Fig. 3 Alkali-activated artificial aggregates production process **a** Dry mixing of raw materials, **b** Alkaline solution, **c** Pelletization, **d** Freshly formed pellets, **e** Pellets after one day of ambient curing, **f** Pellets sealed in plastic bags for 28 days for curing



efficiency, pelletization duration, and pellet characteristics, were considered to optimize the artificial aggregates. In the production of ACA, FA (52.5%), GGBS (32.5%), SSP (15%), and 10 M alkaline solution (F52.5G32.5S15M10) were employed. The alkaline solution was prepared by mixing the Na_2SiO_3 solution with the NaOH solution with a weight ratio of 2:1 (Na_2SiO_3 :NaOH). SSP, along with the higher content of GGBS, showed a unique role in nucleating or agglomerating the raw material particles into pellets in a short duration of 11–8 min; as a result, all obtained pellets got more time to undergo compaction by colliding with one another, and the pelletizer side walls led to pellets of better properties. The aggregates were strengthened by employing ambient curing for 28 days. The artificial aggregate pellets were selected in the 4.75 mm to 20 mm range to carry out the concrete production.

Tests conducted on artificial aggregates

The characteristics of the produced aggregates that the present author has investigated are pertinent to concrete production because the primary goal of manufacturing aggregates is to employ them in concrete production. These characteristics include particle size distribution, specific gravity, bulk density, water absorption, impact strength, and crushing strength. The particle size distribution of aggregates was carried out as per IS 383:2016 [31] and IS 2386 (Part 1):1963 [32]. The specific gravity, bulk density, and water absorption tests were carried out as per IS 2386 (Part 3):1963 [33]. The impact and crushing strength tests were performed according to IS 2386 (Part 4):1963 [34]. The characteristics of produced alkali-activated artificial aggregates were comparable to those of natural coarse aggregates, tabulated in Table 2

Table 2 Characteristics of artificial and natural coarse aggregates

Characteristics	Type of coarse aggregates	
	ACA	NCA
Specific gravity	2.09	2.58
Fineness modulus	6.67	6.77
Loose bulk density (kg/m^3)	1264.17	1383.91
Compacted bulk density (kg/m^3)	1306.32	1543.47
Water absorption (%)	0.75	0.50
Impact value (%)	12.06	23.39
Crushing value (%)	18.49	22.39

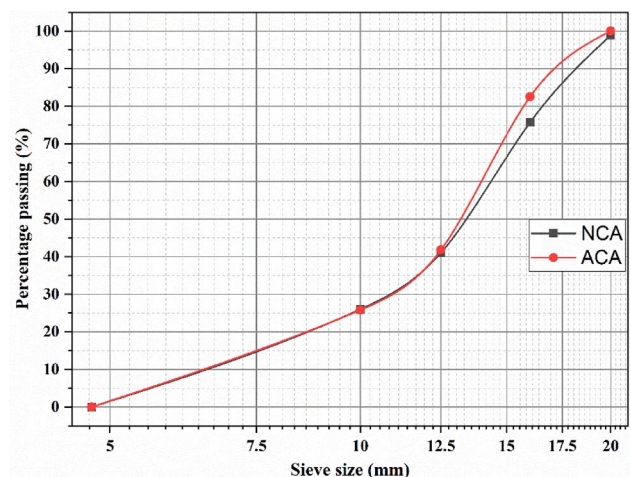


Fig. 4 Gradation of ACA and NCA

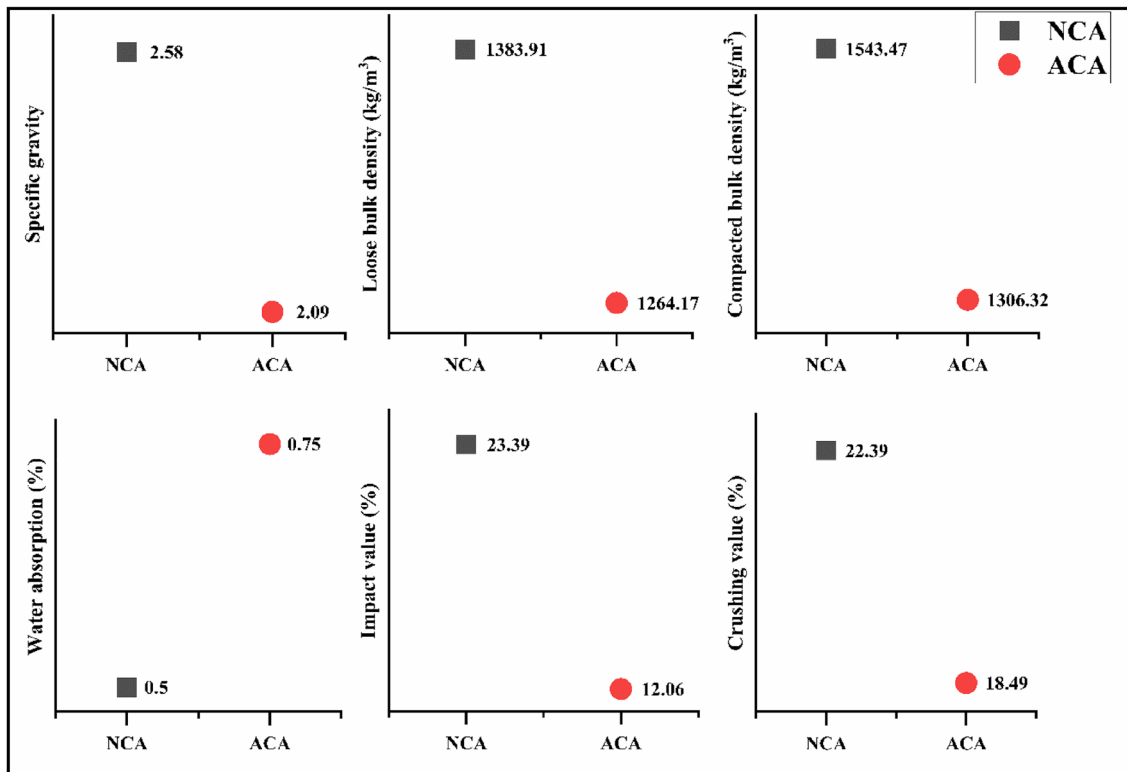


Fig. 5 Physical and mechanical properties of ACA and NCA

and presented in Figs. 4 and 5. It was observed that the specific gravity (2.09) of the ACA obtained was lower than the specific gravities of the raw materials (FA: 2.24, GGBS: 2.85, SSP: 2.36) involved in their production; which might be due to reasons as follows: (i) Geopolymerization is a continuous process. Especially when thermal curing is not done, FA molecules tend to react in a slower phase, making the aggregates stronger in later ages. This slow phase reactivity will also influence the specific gravity. With an increase in age, polymerization increases, which will make the matrix dense and stronger. (ii) Only the centrifugal and gravitational forces have acted on the materials to form aggregates, which cannot significantly improve the specific gravity. (iii) A combination of multiple materials prepares artificial aggregates. The specific gravity of the final product is dependent on the specific gravity of raw materials as well as activation fluid. (iv) An increase in specific gravity can be expected by further effective compaction. Also, an increase in fluid content can enhance specific gravity. Figure 6 represents SEM micrographs of artificial aggregates, and it can be seen that the aggregate surface was dense and impermeable, made with compacted particles. Figure 7 demonstrates the XRD pattern of aggregates and identifies that the formation of gels that include calcium silicate hydrate (C-S-H), sodium aluminosilicate hydrate (N-A-S-H), and calcium aluminosilicate hydrate (C-A-S-H). Hence, produced aggregates

were microstructurally solid and supported aggregates of good qualities, i.e., high strength and low water absorption.

Concrete production

This study produced concrete with alkali-activated artificial and natural coarse aggregates. The ingredients utilized, mix design, and tests conducted on concrete samples are discussed below.

Materials

The OPC 53-grade cement was examined according to IS 269: 2015 [35] and IS 4031 (Part 1, 4, 5, and 6): 1996 [36–39], which had 3.1 specific gravity. It depicted standard consistency at 31% of water content with an initial and final setting time of 52 and 310 min, respectively. With a fineness of 99%, cement depicted a strength of 55 MPa at 28 days. Natural river sand was examined as per IS 383: 2016 [31] and IS 2386 (Part 1 and 3):1963 [32, 33]. It exhibited a specific gravity of 2.62 with 1.2% water absorption. Fine aggregate has a loose bulk density of 1460 kg/m³, and as per the gradation, it satisfied the conditions of Zone II. Hence, it can be used for both plain and reinforced concrete. Natural coarse aggregate procured

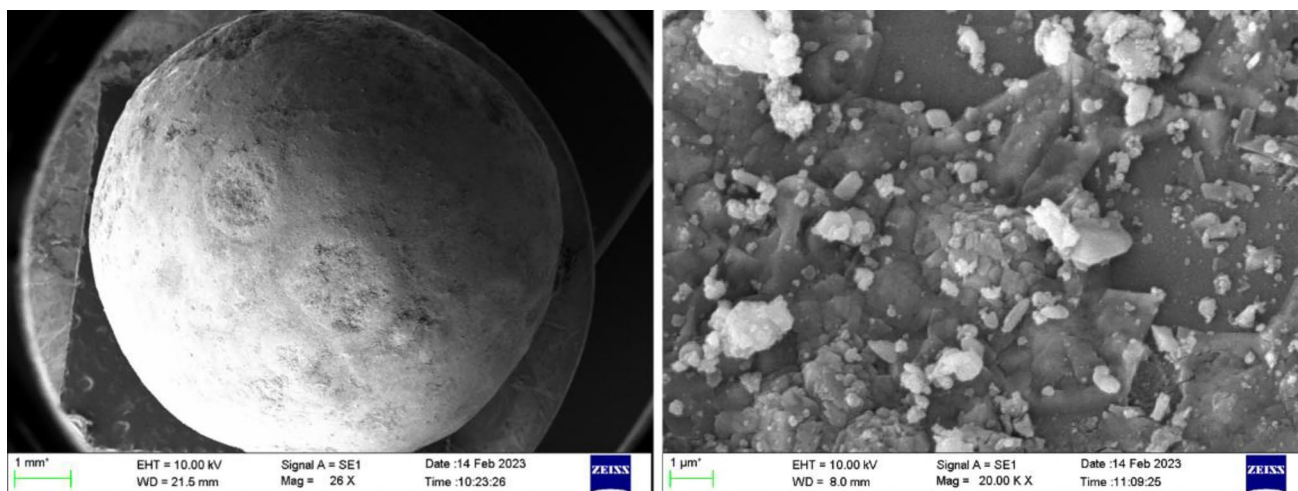


Fig. 6 SEM micrographs of ACA

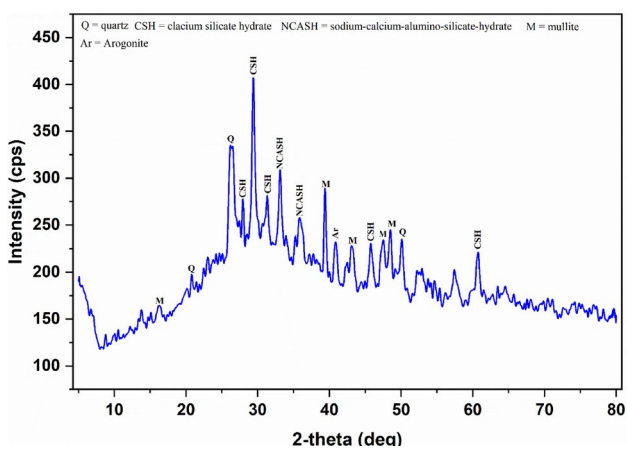


Fig. 7 XRD pattern of ACA

from a local quarry and artificial coarse aggregates produced in a study were used. The physical and mechanical properties were determined according to IS 383: 2016 [31]

and IS 2386 (Part 1, 3, and 4):1963 [32–34]. Table 2 lists the physical and mechanical properties of both NCA and ACA. All the raw materials used for concrete production are shown in Fig. 8.

Mix design

In this study, a mix design was done for M40-grade concrete incorporated with artificial aggregates as per IS 10262: 2019 [40]. In concrete, NCA were replaced with ACA by 25%, 50%, 75%, and 100%. Natural aggregate concrete (NAC) was also produced to perform a comparative study. The w/c ratio for making workable concrete was fixed through trial tests. In view of comparing the performance of concrete mixes, all mix proportioning were designed to attain workability of at least 100 mm slump. Each mix had the same volume proportions; the only difference between them was the quantity of ACA incorporated. Table 3 shows the mixed proportions of artificial aggregate concrete (AAC) and NAC.

Fig. 8 Materials a Concrete ingredients, b Stretched view of ACA



Table 3 Mix design

Mix ID	Contents (kg/m ³)						
	Mix name	OPC	Sand	NCA	ACA	Water	W/C ratio
M1	100% NCA	450	628	1098	–	180	0.40
M2	75% NCA + 25% ACA	450	628	824	222	180	0.40
M3	50% NCA + 50% ACA	450	628	549	445	180	0.40
M4	25% NCA + 75% ACA	450	628	275	667	180	0.40
M5	100% ACA	440	635	–	908	176	0.40

Mixing, casting, and curing

A 150-L pan mixer was used to mix the constituents of the concrete. The aggregates were placed in the mixer first, then the cement. The first 5 min were spent mixing the dry ingredients. After dry mixing, a calculated quantity of water was added to the mixer, and further mixing was carried out until a homogeneous mix was obtained. The mix formed was examined for the fresh property as per IS 1199 (Part 2): 2018 [41] using the slump cone test. Then the mix was filled into molds in three layers with efficient compaction according to IS 516 (Part1/Sec1): 2021 [42] and IS 10086: 1982 [43]. Finally, surface finishing was done to attain a homogeneous, smooth surface. After 24 h, specimens were demoulded and subjected to water immersion curing at room temperature until 7, 14, 28, and 90 days in accordance with Indian standards IS 1199 (Part 5): 2018 [44]. The process of production of concrete by incorporating ACA and casting to a required shape and size carried out in a study has been shown in Fig. 9.

Test procedures

The slump test was conducted according to IS 1199 (Part 2): 2018 [41] as soon as fresh concrete was produced. The fresh and dry density measurements were generally done in accordance with IS 1199 (Part 3): 2018 [45] and IS 516 (Part 2/ sec1): 2018 [46], respectively. Concrete was tested for water permeability in accordance with IS 3085: 1965 [47] at 28 and 90 days. For 72 h, pressurized water (5 ± 0.5 kg/cm²) was forced to enter the 150 mm square sample. At the end of the testing period, the samples were separated from the center, and the maximum depth of water permeability in millimeters was determined. The UPV test was conducted as per IS 516 (Part 5/sec1):2018 [48] at 28 and 90 days to confirm the homogeneity and quality of concrete by passing electronic waves into the concrete sample. The resistance to chloride ion penetration was also conducted on concrete sample sections of 100 mm diameter and 50 mm thick at 28 and 90 days as per ASTM C1202. The sodium chloride solution concentration was 3 M, and a 60 V DC power supply was provided for the



Fig. 9 Concrete production **a** Dry mixing of raw materials, **b** Fresh concrete, **c** Slump measurement, **d** Concrete samples after demoulding

cells. The resistance to chloride ion penetration was determined by measuring charges passed into the concrete sample. The mechanical properties of concrete, such as CS, STS, and FS, were determined as per IS 516 (Part 1/sec1): 2021 [42]. The number of concrete specimens tested for each mechanical property was three ($N=3$); the average of the three values was considered the final strength value. The concrete cubes of $150 \times 150 \times 150$ mm size were considered for measuring the CS. For testing, the specimens were initially removed from the curing tank after 7, 14, 28, and 90 days and kept in the sunlight to attain dryness. The samples were placed on the universal testing machine (UTM) properly, and then the compressive load was applied gradually at the rate of 2.5 KN/sec until the first crack appeared. The STS was also examined on the same equipment at the same ages with cylindrical concrete specimens of 150 mm diameter and 300 mm height. However, FS was checked by placing a 28-day cured beam sample of size $500 \text{ mm} \times 100 \text{ mm} \times 100 \text{ mm}$ in UTM with 2-point load arrangements. The CS, STS, and FS of concrete samples were calculated using the following formulae, and Fig. 10 shows a test setup to measure concrete samples' mechanical and transport properties.

$$f_c = P/A \quad (1)$$

$$f_t = 2P/\pi DL \quad (2)$$

$$f_{fl} = (P \times l)/b \times d^2 \quad (3)$$

(Used when the distance between the line of failure and the nearest support is greater than 13 cm for 10 cm sample).

$$f_{fl} = (3P \times a)/b \times d^2 \quad (4)$$

(Used when the distance between the line of failure and the nearest support is less than 13 cm but greater than 11 cm for 10 cm sample).

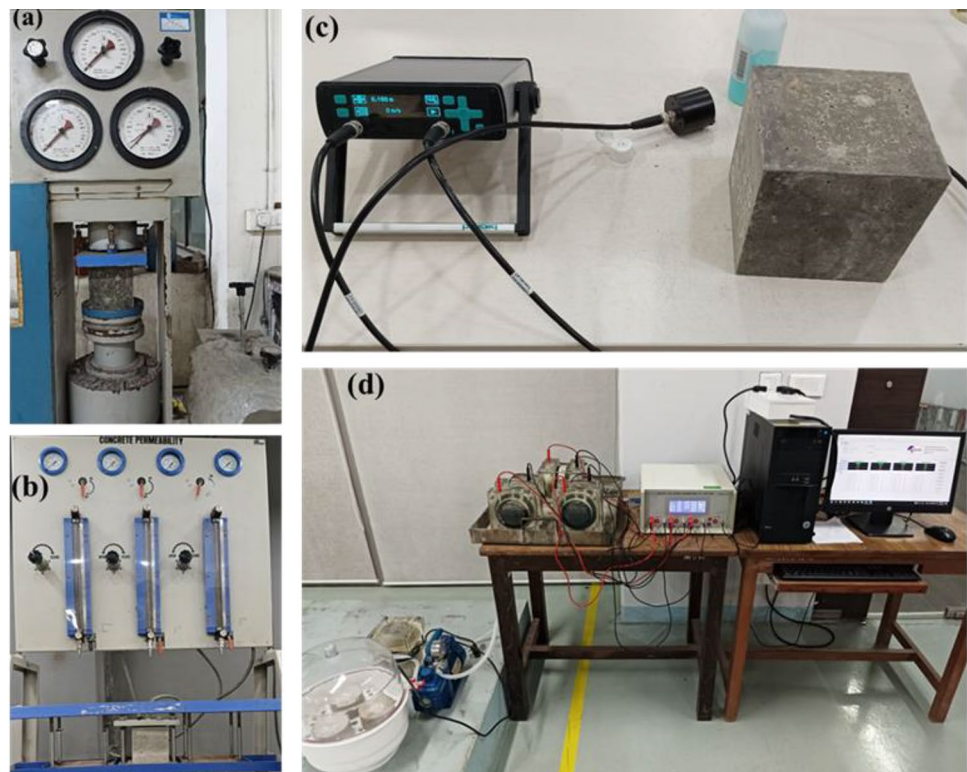
where, f_c = compressive strength (MPa) f_t = Split tensile strength (MPa) f_{fl} = Flexural strength (MPa) P = load value at breakdown of sample (KN) A = area of the sample (mm^2) D = diameter of the sample (mm) L = length of the sample (mm) l = effective span of beam (mm) b = beam width (mm) d = beam depth (mm) a = distance between the line of failure and the nearest support.

Results and discussion

Workability

The workability of the concrete was checked by measuring its slump value, presented in Fig. 11. The concrete was workable, cohesive, and not segregated. All of the concretes had achieved their intended slumps. The results demonstrate

Fig. 10 Test setup **a** Compressive strength, **b** Water permeability, **c** UPV, **d** RCPT



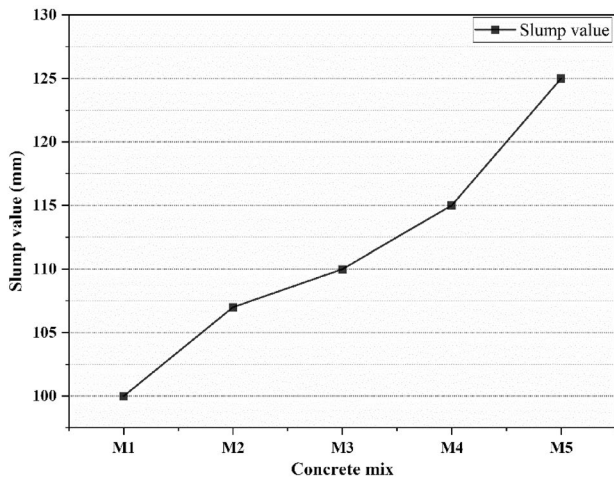


Fig. 11 Workability of concrete mixes

that all AAC combinations had slumps between 107 and 125 mm, while the NAC showed 100 mm. The slump obtained for AAC was somewhat greater than that obtained for NAC for a given w/c ratio. This could result from the spherical shape of artificial aggregates as opposed to the angular particles of natural crushed aggregates, which reduces the water demand for fresh concrete [5, 11, 20, 49–52]. It can also be observed that the workability of concrete increased with the increased percentage replacement of artificial aggregates [53, 54].

Density of concrete

The fresh and air-dry density of the concrete decreased with the increased percentage of replacement of artificial aggregates, and all AACs exhibited lower density than NAC, mainly due to artificial aggregates of lightweight compared to natural crushed aggregates. From Fig. 12, it can be observed that the fresh density of AAC lies in the range of 2171.85–2410.36 kg/m³, and NAC presented 2508.14 kg/m³. The air-dry density of the AAC at 28 and 90 days lies in the range of 2160–2364.44 kg/m³ and 2186.67–2373.33 kg/m³, respectively, while NAC showed 2434.07 kg/m³ and 2462.22 kg/m³. These results indicate that concrete density enhanced with the increased days of curing, which is attributed to the prolonged hydration process forming compact and refined microstructure. Further, it can be revealed that replacing the entire volume of natural aggregates with artificial aggregates can achieve an 11% density reduction.

Compressive strength

The CS is significant because it serves as the primary criterion for determining if a particular concrete mixture will be enough for a given application. The CS of the AAC and

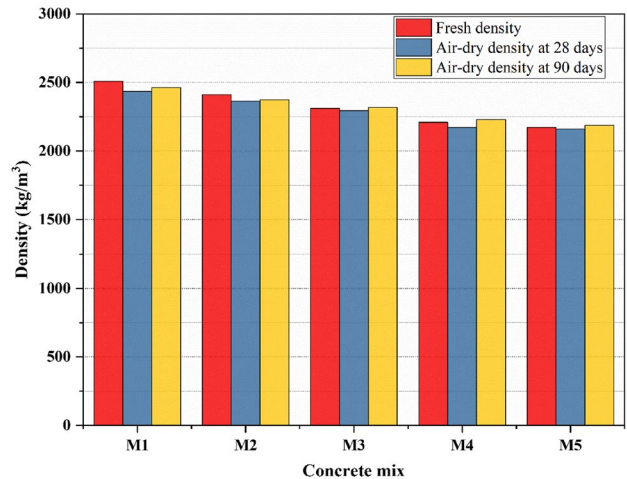


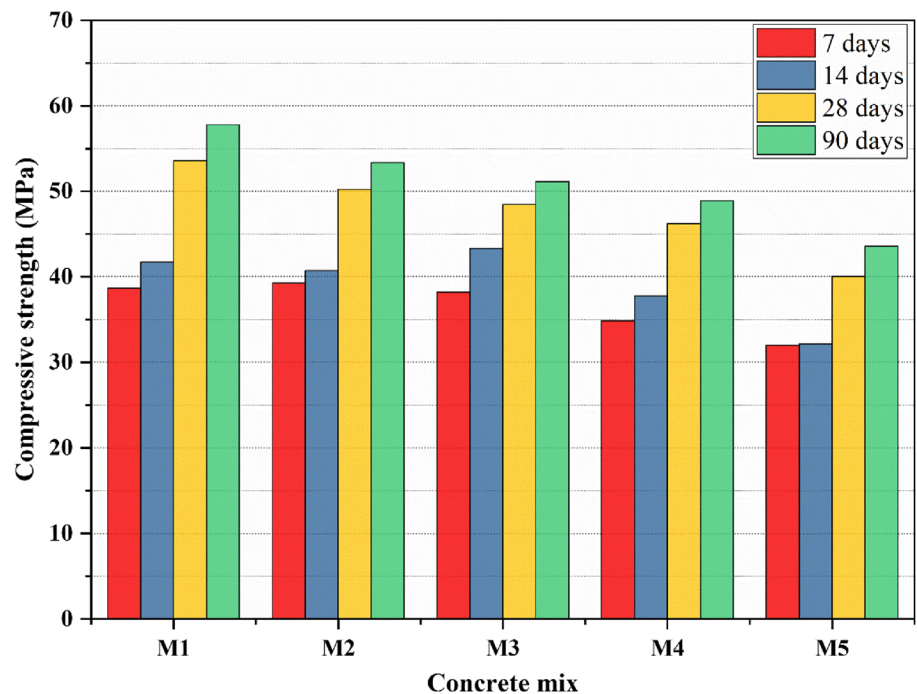
Fig. 12 Density of concrete mixes

NAC for different curing ages is presented in Fig. 13. The CS of all concrete mixes was increased with the increased days of curing. The 28-day CS of AAC ranges from 40.4 MPa to 50.22 MPa, and NAC showed 53.55 MPa. The 90-day CS of AAC ranges from 43.56 MPa to 53.33 MPa, and NAC showed 57.78 MPa. The concrete of mixes M2 and M3 have exhibited a strength comparable to mix M1 made full of natural aggregates (NAC). From the obtained results, it can be observed that the concrete with the increased volume of artificial aggregates showed a reduction in CS, which might be due to artificial aggregates of slightly lower density, higher porosity, and weaker compatibility of spherical shape particles with the angular shape natural aggregates. Similar results can be seen in previous research stating that the increased volume of artificial aggregates in concrete will reduce the strength of the concrete due to aggregates of lower density, higher porosity, and lower strength [5, 11, 29, 49]. Artificial aggregates also have an essential role in improving the strength of concrete with the increased days of curing by enhancing the interfacial transition zone (ITZ) through the mechanical interlocking of the paste matrix into the surface pores of the aggregates [49, 55, 56]. It can also be noticed that the CS of concrete showed a direct relationship with the density, i.e., strength increased with the density of concrete.

Split tensile strength

The bond strength, anchoring, shear resistance, and crack resistance of concrete depend on the STS; the better the STS, the better the structural qualities [5]. Figure 14 shows the results of the STS test at the age of 7, 14, and 28 days. The 28-day STS of the AAC varied from 2.69 MPa to 3.81 MPa, while NAC showed 4.20 MPa. The STS of all concrete mixes followed a similar pattern of results as discussed under

Fig. 13 Compressive strength of concrete mixes on different days of curing



the compressive strength test, i.e., the concrete with the increased volume of artificial aggregates showed a reduction in TS [20]. A similar hypothesis in previous research states that CS and STS have a direct relationship [5, 57]. The artificial aggregates' strength significantly impacts the ultimate strength of concrete [5]. Figure 15 shows the failure pattern of concrete samples under STS. Inspection of broken surfaces revealed that interfacial bond failure had not occurred. For all concretes, it was discovered that the aggregate particles split along the diameter to form two equal half-spheres. After the testing, the bond between the aggregates and the

cured cement mortar was still strong. Similar observation results can be seen in a study done by Dinakar Pasla [5].

Flexural strength

The flexural characteristics of concrete depend primarily on the mortar's characteristics, and the role of aggregates in demonstrating resistance to flexural bending is minimal [20]. The reduced quantity of artificial aggregates in the mix and matrix densification enhances the concrete's structural qualities [20]. The FS characteristics of all concrete mixes at 28 days of curing are presented in Fig. 16. The FS of AAC ranges from 4.51 MPa to 5.17 MPa, while NAC displayed 5.23 MPa. Most interestingly, in this study, all AAC mixes except M5 showed excellent flexural strengths almost comparable to NAC. It could be attributed to either the densified matrix or a strong interfacial zone formed by penetration of cement paste into the surface pores of the aggregates, creating an interlock, withstanding the higher flexure load. Usually, when concrete specimens are subjected to flexural loads, failure occurs along the paste matrix, and aggregates take a minimal part [20]. Figure 17 depicts the flexure failure pattern of the beam specimens and their broken surfaces. In AAC samples, it can be observed that there is a failure of artificial aggregates also, indicating the existence of interlocking between the surface of artificial aggregates and the paste matrix, enhancing the bond between the phases and supporting the concrete to reach higher strength under flexural load.

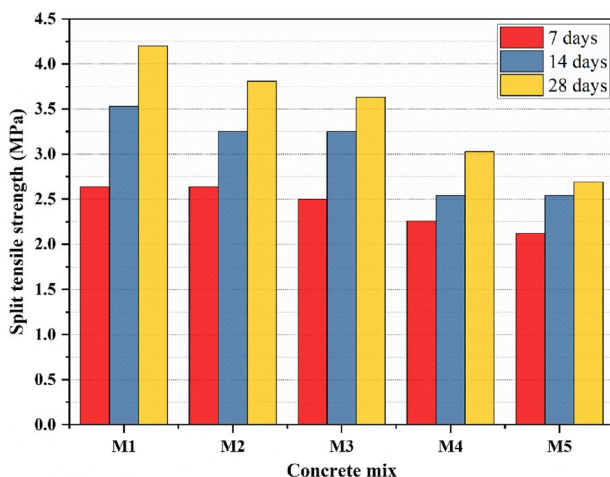


Fig. 14 Split tensile strength of concrete mixes at different days of curing



Fig. 15 Failure of specimens a Failure pattern, b, c broken surfaces

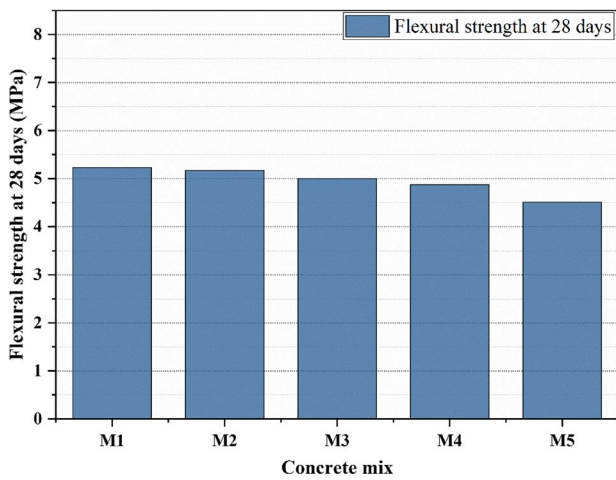


Fig. 16 Flexural strength of concrete mixes at 28 days

Correlation between mechanical properties

Correlation between CS and STS

From an overview of the test data, it is likely to be noted that there is a linear relationship between the results of the CS and STS. The comparison between the obtained results in a study and the relationship found in different standards is shown below [58–60].

$$f_t = 0.59 f_c^{0.5} \text{ (ACI 363)} \tag{5}$$

$$f_t = 0.56 f_c^{0.5} \text{ (ACI 318-14)} \tag{6}$$

$$f_t = 0.3 f_c^{0.66} \text{ (CEB-FIP)} \tag{7}$$

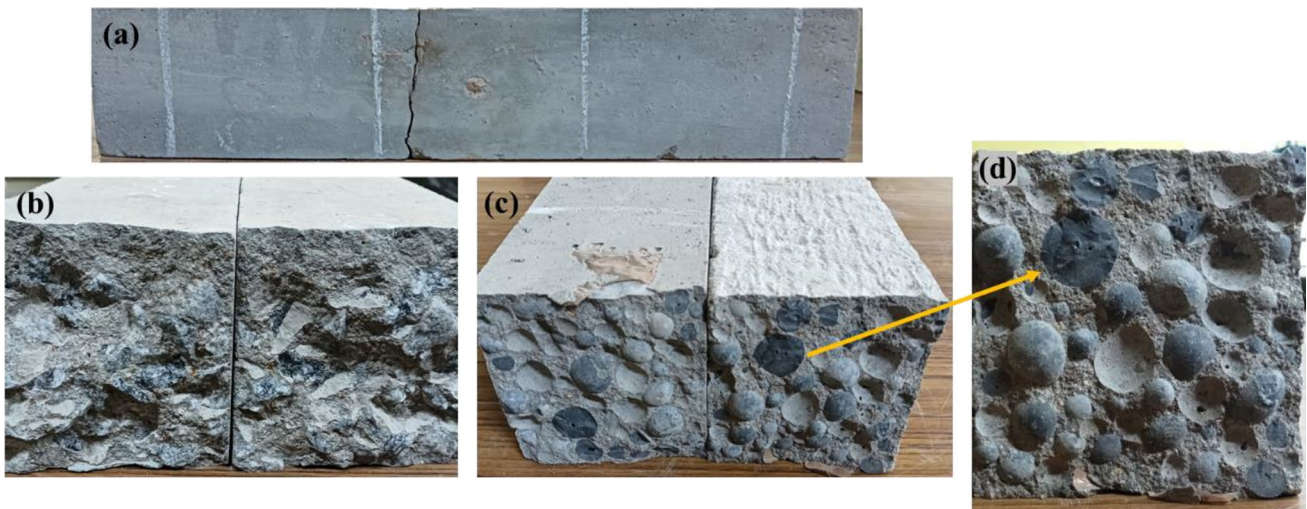


Fig. 17 Failure of specimens a Failure pattern, b AAC's broken surfaces, c, d NAC's broken surfaces

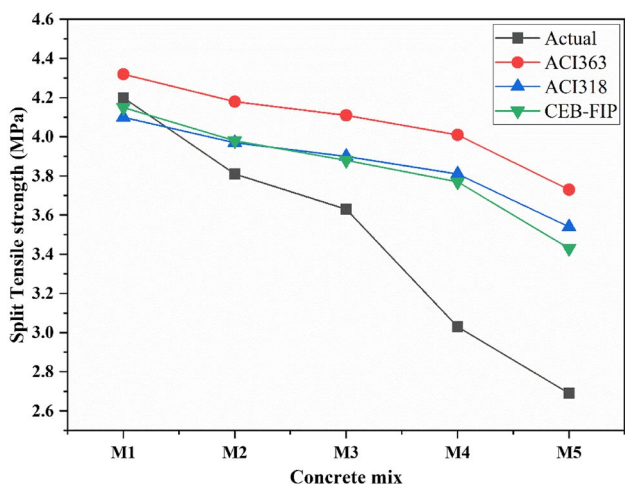


Fig. 18 Correlation between CS and STS

where,

f_t = Split tensile strength (MPa)

f_c = Compressive strength (MPa)

In Fig. 18, the split tensile values that resulted from applying these relationships have been compared with actual values. The values determined by these correlations do not match the actual values except those corresponding to the M1 mix, and there is an average of 15% variance in values. However, some part of the curve follows the trend of relationship suggested in codes. Usually, the aggregates take a significant role in the split tensile test compared to the compression test in which both the aggregates and paste matrix play an essential role. Hence, the variation shown by the AAC mixes with the above correlation values might be attributed to the aggregate’s properties, especially spherical shape, and low density, which had reduced the strength.

Correlation between CS and FS

Similar to the correlation between CS and STS, the flexural strength results obtained in a study are compared with the relationship found in different standards is shown below [59, 61, 62].

$$f_{fl} = 0.7 \sqrt{f_c} \text{ (IS 456-2000)} \tag{8}$$

$$f_{fl} = 0.517 \sqrt{f_c} \text{ (SBC 304)} \tag{9}$$

$$f_{fl} = 0.62 \sqrt{f_c} \text{ (ACI 318-14-2014)} \tag{10}$$

where,

f_{fl} = Flexural strength (MPa)

f_c = Compressive strength (MPa)

In Fig. 19, the flexural strength values that resulted from applying these relationships have been compared with actual values. The values determined by these correlations match the actual values and follow the path given in the codes. It can be observed that the actual values obtained in this study are higher than those obtained from the above correlations and are in line with the values obtained from a correlation suggested by IS 456-2000. The existence of interlocking between the surface of artificial aggregates and the paste matrix enhances the bond between the phases. It supports the concrete to reach higher strength under flexural load.

Ultrasonic pulse velocity

The UPV test is used to check cracks, cavities, and other flaws in concrete, i.e., concrete quality [48, 53, 63, 64]. As per IS 516 (part 5/Sec1): 2018 [48], the concrete can be considered good quality when the UPV values fall between 3.75 and 4.40 km/s, while the concrete is of excellent quality when the values are over 4.40 km/s. Figure 20 shows the UPV of all concrete combinations measured at 28 and 90 days. The AAC exhibited UPV ranges from 3.66 km/s to 4.57 km/s and 3.91 km/s to 4.63 km/s at 28 and 90 days, respectively, while NAC showed 4.87 km/s and 4.98 km/s. From these results, it can be noted that the quality of concrete lies between good and excellent. The increased replacement of NCA with ACA has decreased UPV. The possible causes of this observed decrease in UPV values include the existence of pores, non-homogeneity, and insufficient particle packing [53, 65, 66]. However, the concrete quality was not affected dramatically by adding artificial aggregates. It can also be noticed that the UPV of concrete shows a direct relationship with the density and strength properties; as the density and strength of the concrete rise, then the UPV of concrete also rises, which can be seen in Figs. 21 and 22.

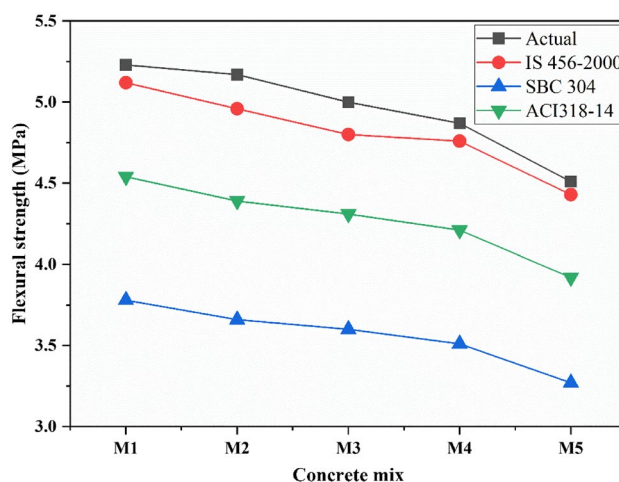


Fig. 19 Correlation between CS and FS

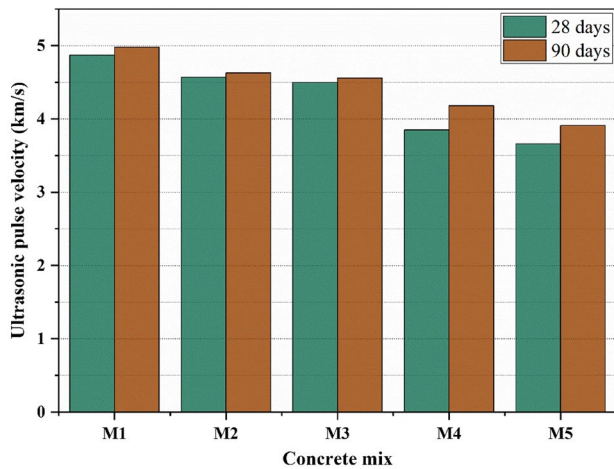


Fig. 20 Ultrasonic pulse velocity of concrete mixes at different days of curing

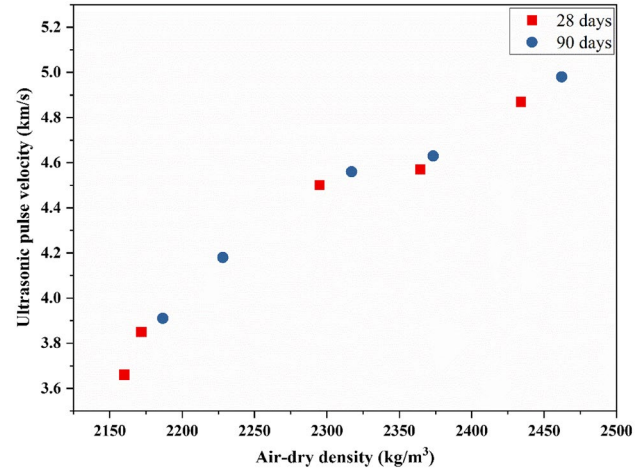


Fig. 22 Relationship between density and ultrasonic pulse velocity for different mixes

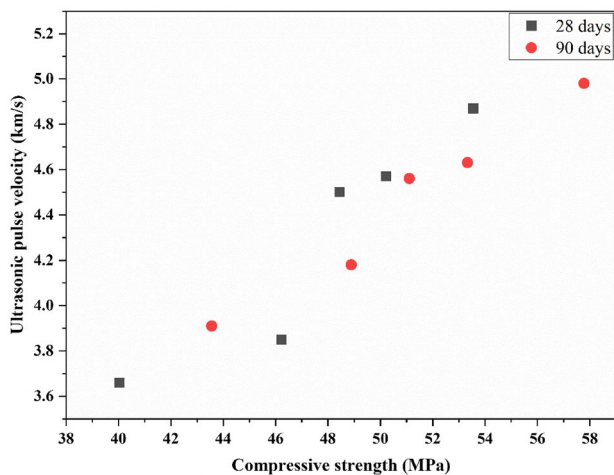


Fig. 21 Relationship between compressive strength and ultrasonic pulse velocity for different mixes

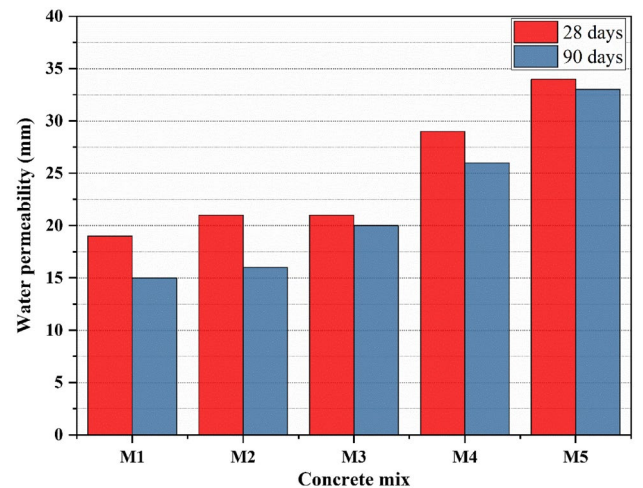


Fig. 23 Water permeability of concrete mixes at different days of curing

Water permeability

The water permeability of all concrete mixes is presented in Fig. 23. The concrete mixes M1, M2, M3, M4, and M5 showed water permeabilities of 19 mm, 21 mm, 21 mm, 29 mm, and 34 mm, respectively, at 28 days and 16 mm, 15 mm, 20 mm, 26 mm, and 33 mm at 90 days. The concrete mixes of type M1 and M2 showed almost comparable water permeabilities. The results suggested that the water permeability was reduced as the curing age was increased from 28 to 90 days [49]. The water permeability for ACA mixes was higher than NAC (M1) mix for the same w/c ratio; a similar pattern of results can be seen in a study done by Jignesh Kumar Patel et al. [49]. It could be attributed to more mortar matrix occupied in the wider space left between the

aggregates of spherical shape, which can be seen in Figs. 15 and 17, allowing water to penetrate through it. Further, the aggregates of minor porous nature extend this depth of penetration. However, water permeability has reduced as the days of curing have increased, making the matrix densified and refined. Additionally, Figs. 24 and 25 show that the water permeability has an inverse relationship with CS and density, respectively, i.e., water permeability reduced as the CS and density increased.

Rapid chloride penetration

The movement of chloride ions within the concrete matrix is assessed using a rapid chloride penetration test (RCPT). The curing age and lower water-binder ratio improve the

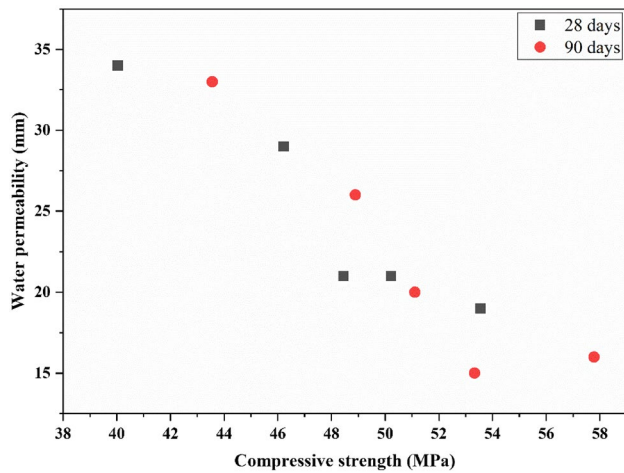


Fig. 24 Relationship between compressive strength and water permeability for different mixes

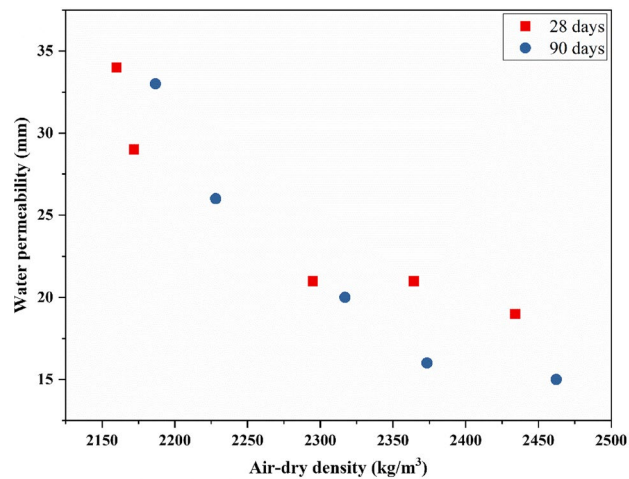


Fig. 25 Relationship between density and water permeability for different mixes

resistance to chloride penetration in concrete. Additionally, it depends on the kind of binder used in the matrix [5, 11, 49, 67, 68]. In AAC, curing age has a greater impact than water/binder ratio and binder type; as curing time increases, chloride penetration decreases as a result of improved pore structure [5, 49, 67]. The chloride ion penetration of all concrete mixes carried out in a study is depicted in Fig. 26. According to ASTM C1202, all concrete combinations showed minor and minimal RCPT values at 28 and 90 days, respectively. Like water permeability results, the chloride ion penetration results improved as the curing age increased from 28 to 90 days. Additionally, it can be observed that the RCPT value also has an inverse relationship with CS and density, demonstrating that the RCPT value reduced as the CS and dry density increased, which can be seen in Figs. 27 and

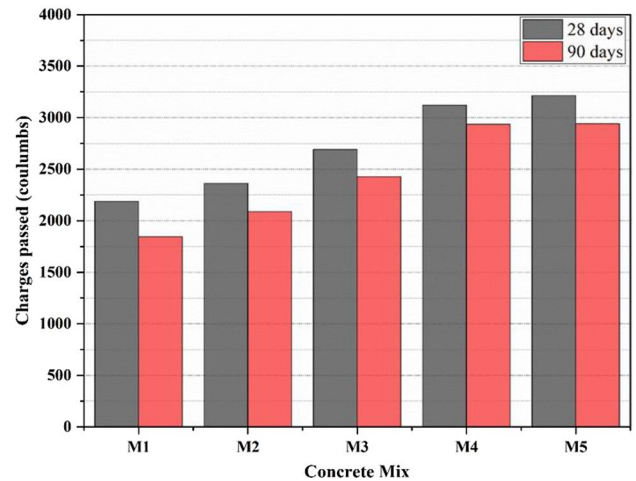


Fig. 26 Chloride ion penetration of concrete mixes at different days of curing

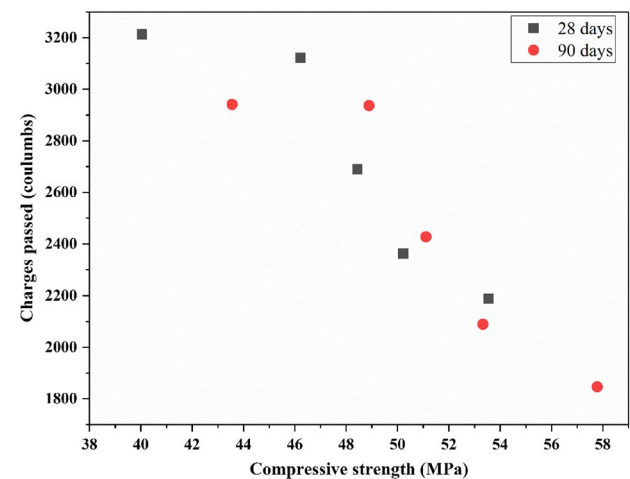


Fig. 27 Relationship between compressive strength and chloride ion penetration for different mixes

28, respectively. NAC (M1) exhibited considerably lower chloride permeability than AAC for the same water/binder ratio, which could be attributed to the natural aggregate's lower water absorption.

Microstructure

ITZ

The image shown in Fig. 29 represents the ITZ. The cement matrix and interface of all concrete did not significantly differ from one another. The cement paste appears to be the same color in all samples and has a consistent, solid microstructure. Additionally, it was noted that the ITZ showed

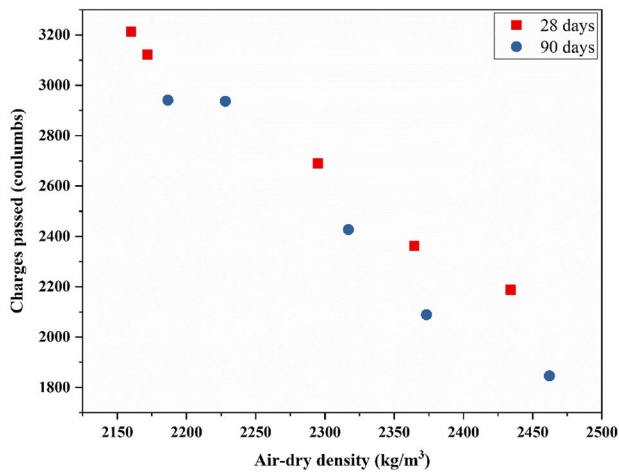


Fig. 28 Relationship between density and chloride ion penetration for different mixes

strong bonding between the two phases. The interface and cement paste showed almost no signs of microcracking. The ITZ becomes more compact and is of higher quality due to the formation of stable compounds by chemical reactions between binders and aggregates. This is also obvious with concrete's CS improving. Further, the ITZ between the natural aggregate and the hardened cement paste (HCP) shows the “Wall effect” or “Surface effect” that occurs at the natural aggregate's surface. In AAC, the cement paste avoids the “Wall Effect” on the ITZ, which reduces porosity by penetrating the artificial aggregate surface pores to a certain depth. The surface pores offer the interlocking site for cement paste to create a better interfacial bond at the ITZ, leading to an enhanced strength comparable to natural aggregate concrete [55, 56, 69]. Further, the degree of alkalinity of the artificial aggregate influences the ITZ of concrete. The degree of alkalinity depends on the molarity of the activator solution. As the molarity increases, the

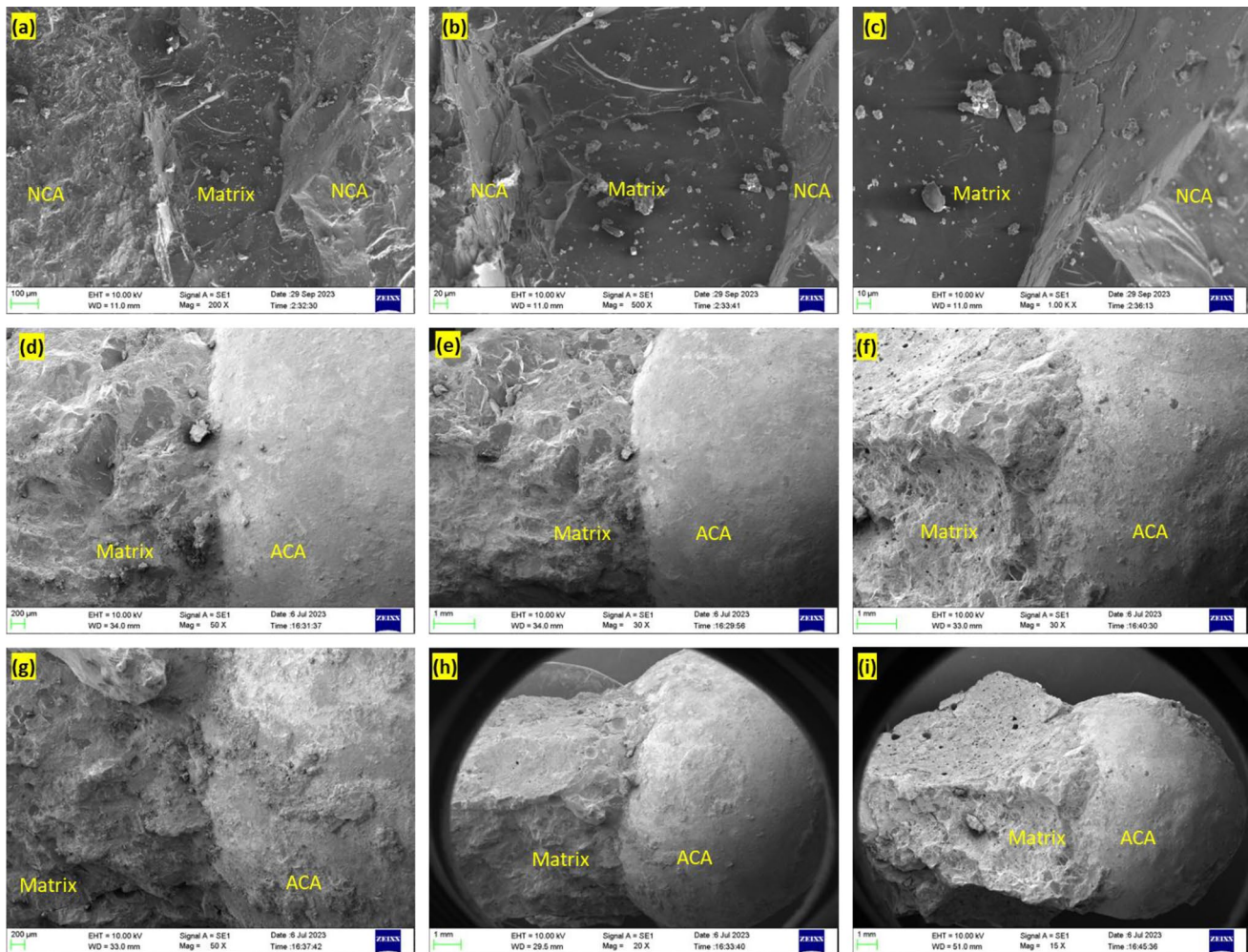


Fig. 29 SEM micrographs of concrete mixes a–c M1, d M2, e M3, f M4, g M5, h, i M4

strength of the material increases, which, in turn, enhances the end product's strength [9, 70–72].

XRD

The XRD patterns for concrete mixes M2, M3, M4, and M5 are shown in Fig. 30. These XRD patterns did not noticeably differ from one another, proving that the mineralogical composition of concrete was not changed by adding artificial aggregates to it. Quartz and minerals containing calcium, aluminosilicate, and hydroxide were found to have prominent peaks, showing that the main mineral phases in the concrete are quartz, calcium silicate hydrate, calcium hydroxide, ettringite, calcite, kyanite, and portlandite. The peak of quartz is attributed to sand and aggregates, whereas the peak of calcium-bearing minerals is attributed to cement. Even though a substantial amount of C-S-H had been identified in the concrete, it was chemically reactive and one of the primary cement-hydrated products, which helped the concrete acquire its strength.

Conclusions

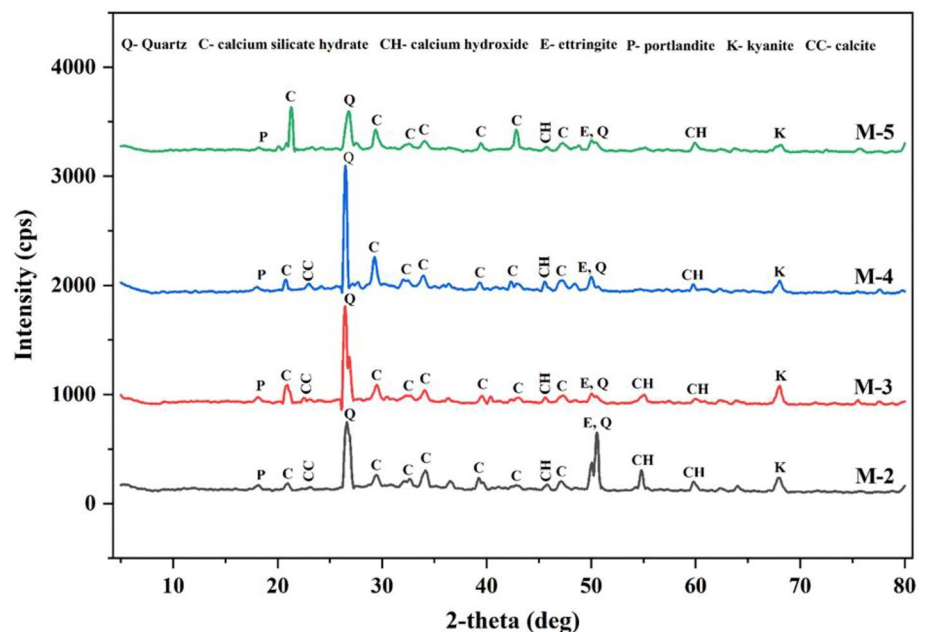
The following conclusions can be made from the findings and observations of this study:

1. The cold-bonding technique used in this study to manufacture alkali-activated artificial aggregates helps reduce energy consumption and increases the practical use of artificial aggregates. In addition, it promotes the use of various waste products in manufacturing aggregates.

Based on the above findings, it was determined that artificial aggregates could be utilized to make structural concrete.

2. The workability of concrete increases with the increased addition of artificial aggregates at a given water-cement ratio due to aggregates of spherical shape demanding less water for internal friction. Concrete density decreases with the increased replacement level of artificial aggregates; the self-weight of concrete can be reduced, resulting in cost reduction.
3. The compressive strength of concrete incorporated with artificial aggregates ranges between 40.4 and 50.22 MPa at 28 days and 43.56–53.33 MPa at 90 days with normal water curing, suggesting that the concretes can be employed for structural purposes. The split tensile strength of artificial aggregate concrete ranges between 2.69 and 3.81 MPa. The fact that there was almost no interfacial bond failure on the split surface of the specimens was confirmed by SEM microstructural analysis on the interfacial zone, which revealed a homogenous, nonporous, and robust interface bonding between the aggregates and cement paste.
4. The quality of the artificial aggregate concrete measured in ultrasonic pulse velocity ranges between good to excellent, comparable to natural aggregate concrete, and enhanced with the age of curing. Further, the resistance to water absorption and chloride ion penetration also enhanced with the increased age of curing attributed to the refinement of pore structure, and the concrete with natural aggregate performed slightly better than concrete with artificial one due to natural aggregates' lower water absorption making concrete less porous.

Fig. 30 XRD patterns of concrete mixes at 28 days of curing



5. The density, strength, ultrasonic pulse velocity, water permeability, and chloride ion penetration of concrete are correlated. The water permeability and chloride ion penetration results presented an inverse relationship with the strength and density of concrete, whereas the ultrasonic pulse velocity showed a direct relationship.
6. The interfacial transition zone formed between the cement paste and aggregate phase is strong, compact, and free from microcracks due to the formation of reaction products and penetration of cement paste into the aggregates' surface pores, developing a mechanical interlocking between the surface of aggregate and cement paste. The addition of artificial aggregates to concrete has not changed the mineralogical composition of the concrete, and the production of a significant amount of hydrated product C-S-H helps concrete obtain strength.

The production of artificial aggregates through waste recycling offers an environmentally friendly approach to waste management and an efficient replacement for the natural aggregates extracted from natural deposits. As a result, using artificial aggregates let the building industry be sustained for a longer time.

Funding Open access funding provided by Manipal Academy of Higher Education, Manipal.

Open Access This article is licensed under a Creative Commons Attribution 4.0 International License, which permits use, sharing, adaptation, distribution and reproduction in any medium or format, as long as you give appropriate credit to the original author(s) and the source, provide a link to the Creative Commons licence, and indicate if changes were made. The images or other third party material in this article are included in the article's Creative Commons licence, unless indicated otherwise in a credit line to the material. If material is not included in the article's Creative Commons licence and your intended use is not permitted by statutory regulation or exceeds the permitted use, you will need to obtain permission directly from the copyright holder. To view a copy of this licence, visit <http://creativecommons.org/licenses/by/4.0/>.

References

1. Shivaprasad KN, Das BB, Krishnadas S (2021) Effect of curing methods on the artificial production of fly ash aggregates. In: lecture notes in civil engineering. Springer science and business media Deutschland GmbH 23–32
2. Shivaprasad KN, Das BB (2021) Study on the production factors in the process of production and properties of fly ash-based coarse aggregates. *Adv Civ Eng*. <https://doi.org/10.1155/2021/4309569>
3. Shivaprasad KN, Das BB (2018) Determination of optimized geopolymerization factors on the properties of pelletized fly ash aggregates. *Constr Build Mater* 163:428–437. <https://doi.org/10.1016/j.conbuildmat.2017.12.038>
4. Ul Rehman M, Rashid K, Ul Haq E, Hussain M, Shehzad N (2020) Physico-mechanical performance and durability of artificial lightweight aggregates synthesized by cementing and geopolymerization. *Constr Build Mater* 232:117290. <https://doi.org/10.1016/j.conbuildmat.2019.117290>
5. Dinakar P (2013) Properties of fly-ash lightweight aggregate concretes. *Proceedings of Institution of Civil Engineers: Constr Mater* 166:133–140. <https://doi.org/10.1680/coma.11.00046>
6. Bhandary RP, Rao AU, Shetty PP, Blesson S, Thomas BS (2023) Application of coffee husk ash as partial replacement of fine aggregate in concrete. *Sustainability* 15:13328. <https://doi.org/10.3390/su151813328>
7. Qian L-P, Xu L-Y, Alrefaei Y, Wang T, Ishida T, Dai J-G (2022) Artificial alkali-activated aggregates developed from wastes and by-products: a state-of-the-art review. *Resour Conserv Recycl* 177:105971. <https://doi.org/10.1016/j.resconrec.2021.105971>
8. Tian K, Wang Y, Hong S, Zhang J, Hou D, Dong B, Xing F (2021) Alkali-activated artificial aggregates fabricated by red mud and fly ash: performance and microstructure. *Constr Build Mater* 281:122552. <https://doi.org/10.1016/j.conbuildmat.2021.122552>
9. Risdanareni P, Villagran Y, Schollbach K, Wang J, De Belie N (2020) Properties of alkali activated lightweight aggregate generated from Sidoarjo Volcanic Mud (Lusi): fly ash, and municipal solid waste incineration bottom ash. *Mater* 13:2528. <https://doi.org/10.3390/ma13112528>
10. Terzić A, Pezo L, Mitić V, Radojević Z (2015) Artificial fly ash based aggregates properties influence on lightweight concrete performances. *Ceram Int* 41:2714–2726. <https://doi.org/10.1016/j.ceramint.2014.10.086>
11. Kockal NU, Ozturan T (2010) Effects of lightweight fly ash aggregate properties on the behavior of lightweight concretes. *J Hazard Mater* 179:954–965. <https://doi.org/10.1016/j.jhazmat.2010.03.098>
12. Blesson S, Rao AU (2023) Agro-industrial-based wastes as supplementary cementitious or alkali-activated binder material: a comprehensive review. *Innov Infrastruct Solut*. <https://doi.org/10.1007/s41062-023-01096-8>
13. Blesson S, Rao AU, Bhandary RP, Shetty PP, Thomas BS (2023) Comparative characteristics assessment of calcined and uncalcined agro-based waste ash with GGBS and its application in an alkali-activated binder system. *Cogent Eng* 10:2220483. <https://doi.org/10.1080/23311916.2023.2220483>
14. Risdanareni P, Schollbach K, Wang J, De Belie N (2020) The effect of NaOH concentration on the mechanical and physical properties of alkali activated fly ash-based artificial lightweight aggregate. *Constr Build Mater* 259:119832. <https://doi.org/10.1016/j.conbuildmat.2020.119832>
15. Tuan BLA, Hwang CL, Lin KL, Chen YY, Young MP (2013) Development of lightweight aggregate from sewage sludge and waste glass powder for concrete. *Constr Build Mater* 47:334–339. <https://doi.org/10.1016/j.conbuildmat.2013.05.039>
16. Thomas J, Harilal B (2015) Properties of cold bonded quarry dust coarse aggregates and its use in concrete. *Cem Concr Compos* 62:67–75. <https://doi.org/10.1016/j.cemconcomp.2015.05.005>
17. Khan Baykal G, Gü A, Ven D (2000) Utilization of fly ash by pelletization process; theory, application areas and research results. *Turkey* 30(1):59–77
18. Harikrishnan KI, Ramamurthy K (2006) Influence of pelletization process on the properties of fly ash aggregates. *Waste Manage* 26:846–852. <https://doi.org/10.1016/j.wasman.2005.10.012>
19. Vasugi V, Ramamurthy K (2014) Identification of admixture for pelletization and strength enhancement of sintered coal pond ash aggregate through statistically designed experiments. *Mater Des* 60:563–575. <https://doi.org/10.1016/j.matdes.2014.04.023>
20. Gomathi P, Sivakumar A (2015) Accelerated curing effects on the mechanical performance of cold bonded and sintered fly ash aggregate concrete. *Constr Build Mater* 77:276–287. <https://doi.org/10.1016/j.conbuildmat.2014.12.108>

21. Ramamurthy K, Harikrishnan KI (2006) Influence of binders on properties of sintered fly ash aggregate. *Cem Concr Compos* 28:33–38. <https://doi.org/10.1016/j.cemconcomp.2005.06.005>
22. Vasugi V, Ramamurthy K (2014) Identification of design parameters influencing manufacture and properties of cold-bonded pond ash aggregate. *Mater Des* 54:264–278. <https://doi.org/10.1016/j.matdes.2013.08.019>
23. Gomathi P, Sivakumar A (2012) Characterization on the strength properties of pelletized fly ash aggregate. *ARPN J Engg Appl Sci* 7:1523–1532
24. Manikandan R, Ramamurthy K (2008) Effect of curing method on characteristics of cold bonded fly ash aggregates. *Cem Concr Compos* 30:848–853. <https://doi.org/10.1016/j.cemconcomp.2008.06.006>
25. Xu LY, Qian LP, Huang BT, Dai JG (2021) Development of artificial one-part geopolymers lightweight aggregates by crushing technique. *J Clean Prod* 315:128200. <https://doi.org/10.1016/j.jclepro.2021.128200>
26. Sun Y, Li J, Shan, Chen Z, Xue Q, Sun Q, Zhou Y, Chen X, Liu L, Poon CS, (2021) Production of lightweight aggregate ceramsite from red mud and municipal solid waste incineration bottom ash: mechanism and optimization. *Constr Build Mater* 287:122993. <https://doi.org/10.1016/j.conbuildmat.2021.122993>
27. Giro-Paloma J, Mañosa J, Maldonado-Alameda A, Quina MJ, Chimenos JM (2019) Rapid sintering of weathered municipal solid waste incinerator bottom ash and rice husk for lightweight aggregate manufacturing and product properties. *J Clean Prod* 232:713–721. <https://doi.org/10.1016/j.jclepro.2019.06.010>
28. Tajra F, Elrahman MA, Chung SY, Stephan D (2018) Performance assessment of core-shell structured lightweight aggregate produced by cold bonding pelletization process. *Constr Build Mater* 179:220–231. <https://doi.org/10.1016/j.conbuildmat.2018.05.237>
29. Bui LAT, Hwang CL, Chen CT, Lin KL, Hsieh MY (2012) Manufacture and performance of cold bonded lightweight aggregate using alkaline activators for high performance concrete. *Constr Build Mater* 35:1056–1062. <https://doi.org/10.1016/j.conbuildmat.2012.04.032>
30. Bureau of Indian Standards 2013IS 3812 (Part 1): 2013 Pulverized Fuel Ash—Specification, Part 1 For Use as Pozzolana in Cement Mortar and Concrete
31. Bureau of Indian Standards (2016) IS 383: 2016 Coarse and fine aggregate for concrete,—Specification
32. Bureau of Indian Standards (1963) IS 2386 (Part 1): 1963 Methods of test for aggregates for concrete, part 1 particle size and shape
33. Bureau of Indian Standards (1963) IS 2386 (Part 3): 1963 Methods of test for aggregates for concrete, part 3 specific gravity, density, voids, absorption, and bulking
34. Bureau of Indian Standards (1963) IS 2386 (Part 4): 1963 Methods of test for aggregates for concrete, part 4 mechanical properties
35. Bureau of Indian Standards (2015) IS 269: 2015 Ordinary portland cement-specification
36. Bureau of Indian Standards (1996) IS 4031 (Part 1): 1996 Method of physical tests for hydraulic cement, part 1: determination of fineness by dry sieving
37. Bureau of Indian Standards (1988) IS 4031 (Part 5): 1988 Method of physical tests for hydraulic cement, part 5 determination of initial and final setting times
38. Bureau of Indian Standards (1988) IS 4031 (Part 4): 1988 Method of physical tests for hydraulic cement, part 4: determination of consistency of standard cement paste
39. Bureau of Indian Standards (1988) IS 4031 (Part 6): 1988 Method of physical tests for hydraulic cement, part 6: determination of compressive strength of hydraulic cement other than masonry cement
40. Bureau of Indian Standards (2019) IS 10262: 2019 Concrete mix proportioning—guidelines
41. Bureau of Indian Standards (2018) IS 1199 (Part 2): 2018 Fresh concrete - methods of sampling, testing, and analysis, part 2: determination of consistency of fresh concrete
42. Bureau of Indian Standards 2021IS 516 (Part 1/Sec1): 2021 Hardened Concrete—methods of test, part 1: testing of strength of hardened concrete, section1 compressive flexural and split tensile strength
43. Bureau of Indian Standards (2021) IS 10086: 2021 Moulds for use in tests of cement, concrete and pozzolana—specification
44. Bureau of Indian Standards (2018) IS 1199 (Part 5): 2018 Fresh concrete—methods of sampling, testing, and analysis, part 5: making and curing of test specimens
45. Bureau of Indian Standards (2018) IS 1199 (Part 3): 2018 Fresh concrete - methods of sampling, testing and analysis, part 3: determination of density of fresh concrete
46. Bureau of Indian Standards (2018) IS 516 (Part 2/sec1): 2018 Hardened concrete—methods of test, part 2: properties of hardened concrete other than strength, section1: density of hardened concrete and depth of water penetration under pressure
47. Bureau of Indian Standards (1965) IS 3085: 1965 Method of test for permeability of cement mortar and concrete
48. Bureau of Indian standards (2018) IS 516 (Part 5/sec1): 2018 Hardened concrete—methods of test, part 5: non-destructive testing of concrete, section1 ultrasonic pulse velocity testing
49. Patel J, kumar, Patil H, Patil Y, Vesmawala G, (2018) Production and performance of alkali-activated cold-bonded lightweight aggregate in concrete. *J Build Eng* 20:616–623. <https://doi.org/10.1016/j.jobe.2018.09.012>
50. Kou SC, Lee G, Poon CS, Lai WL (2009) Properties of lightweight aggregate concrete prepared with PVC granules derived from scraped PVC pipes. *Waste Manage* 29:621–628. <https://doi.org/10.1016/j.wasman.2008.06.014>
51. Gunning PJ, Hills CD, Carey PJ (2009) Production of lightweight aggregate from industrial waste and carbon dioxide. *Waste Manage* 29:2722–2728. <https://doi.org/10.1016/j.wasman.2009.05.021>
52. Liu X, Chia KS, Zhang MH (2011) Water absorption, permeability, and resistance to chloride-ion penetration of lightweight aggregate concrete. *Constr Build Mater* 25:335–343. <https://doi.org/10.1016/j.conbuildmat.2010.06.020>
53. Satpathy HP, Patel SK, Nayak AN (2019) Development of sustainable lightweight concrete using fly ash cenosphere and sintered fly ash aggregate. *Constr Build Mater* 202:636–655. <https://doi.org/10.1016/j.conbuildmat.2019.01.034>
54. Nadesan MS, Dinakar P (2017) Mix design and properties of fly ash waste lightweight aggregates in structural lightweight concrete. *Constr Mater* 7:336–347. <https://doi.org/10.1016/j.cscm.2017.09.005>
55. Kwek SY, Awang H, Cheah CB, Mohamad H (2022) Development of sintered aggregate derived from POFA and silt for lightweight concrete. *J Build Eng* 49:104039. <https://doi.org/10.1016/j.jobe.2022.104039>
56. Lo TY, Cui HZ (2004) Effect of porous lightweight aggregate on strength of concrete. *Mater Lett* 58:916–919. <https://doi.org/10.1016/j.matlet.2003.07.036>
57. Chang T-P, Prof A, Shieh M-M (1996) Fracture properties of lightweight concrete. *Cem Concr Res* 26(2):181–188
58. ACI 363.2R-98 (1998) Guide to quality control and testing of high-strength concrete reported by ACI committee 363
59. ACI 318-14 (2014) Building code requirements for structural concrete (ACI 318-14) commentary on building code requirements for structural concrete (ACI 318R-14)
60. Euro- International committee for concrete and international federation for prestressing (1990) CEB-FIP model code 1990

61. Bureau of Indian Standards (2000) IS 456: 2000 Plain and reinforced concrete—code of practice
62. SBC 304 (2007) Saudi building code concrete structural requirements
63. Yap SP, Alengaram UJ, Jumaat MZ (2013) Enhancement of mechanical properties in polypropylene- and nylon-fibre reinforced oil palm shell concrete. *Mater Des* 49:1034–1041. <https://doi.org/10.1016/j.matdes.2013.02.070>
64. Liu MYJ, Alengaram UJ, Jumaat MZ, Mo KH (2014) Evaluation of thermal conductivity, mechanical and transport properties of lightweight aggregate foamed geopolymer concrete. *Energy Build* 72:238–245. <https://doi.org/10.1016/j.enbuild.2013.12.029>
65. Chinnu SN, Minnu SN, Bahurudeen A, Senthilkumar R (2021) Recycling of industrial and agricultural wastes as alternative coarse aggregates: a step towards cleaner production of concrete. *Constr Build Mater* 287:123056. <https://doi.org/10.1016/j.conbuilmat.2021>
66. Tanaka CJ, Mohd. Sam AR, Abdul Shukor Lim N, Awang AZ, Hamzah N, Loo P, (2020) Properties of concrete containing blended cement and lightweight artificial aggregate. *Malays J.Civ Eng* 32:59–68. <https://doi.org/10.11113/mjce.v32n2.629>
67. Nadesan MS, Dinakar P (2018) Influence of type of binder on high-performance sintered fly ash lightweight aggregate concrete. *Constr Build Mater* 176:665–675. <https://doi.org/10.1016/j.conbuilmat.2018.05.057>
68. Güneyisi E, Gesoğlu M, Pürsünlü Ö, Mermerdaş K (2013) Durability aspect of concretes composed of cold bonded and sintered fly ash lightweight aggregates. *Compos B Eng* 53:258–266. <https://doi.org/10.1016/j.compositesb.2013.04.070>
69. Barnes BD, Diamond S, Dolch WL (1978) Micromorphology of the interfacial zone around aggregates in portland cement mortar. West Lafayette, Indiana
70. Razak RA, Abdullah MMAB, Hussin K, Ismail KN, Hardjito D, Yahya Z (2015) Optimization of NaOH molarity, LUSI mud/alkaline activator, and Na₂SiO₃/NaOH ratio to produce lightweight aggregate-based geopolymer. *Int J Mol Sci* 16:11629–11647. <https://doi.org/10.3390/ijms160511629>
71. Bekkeri GB, Shetty KK, Nayak G (2023) Producing of alkali-activated artificial aggregates by pelletization of fly ash, slag, and seashell powder. *Innov Infrastruct Solut* 8:258. <https://doi.org/10.1007/s41062-023-01227-1>
72. Bekkeri GB, Shetty KK, Nayak G (2023) Synthesis of artificial aggregates and their impact on performance of concrete: a review. *J Mater Cycles Waste Manag* 25:1988–2011. <https://doi.org/10.1007/s10163-023-01713-9>

Publisher's Note Springer Nature remains neutral with regard to jurisdictional claims in published maps and institutional affiliations.